J Mater Sci: Mater Med (2011) 22:647–656
DOI 10.1007/s10856-011-4241-7

In vivo performance of bilayer hydroxyapatite scaffolds for bone tissue regeneration in the rabbit radius

Teja Guda · John A. Walker · Beth E. Pollot · Mark R. Appleford · Sunho Oh · Joo L. Ong · Joseph C. Wenke

Received: 20 September 2010 / Accepted: 14 January 2011 / Published online: 2 February 2011

Abstract The objective of this study was to investigate the in vivo biomechanical performance of bone defects implanted with novel bilayer hydroxyapatite (HAp) scaffolds that mimic the cortical and cancellous organization of bone. The scaffolds maintained architectural continuity in a rabbit radius segmental defect model and were compared to an untreated defect group (negative control) and autologous bone grafts (positive control). Micro-CT evaluations indicated total bone and scaffold volume in the experimental group was significantly greater than the defect group but lesser than the autologous bone graft treatment. The flexural toughness of the scaffold and the autograft groups was significantly greater than the flexural toughness of the defect group. Interestingly, the absolute density of the bone mineral as well as calcium to phosphorus (Ca/P) ratio in that mineral for the scaffold and autograft contralateral bones was significantly higher than those for the defect contralaterals suggesting that the scaffolds contributed to calcium homeostasis. It was concluded from this study that new bone regenerated in the bilayer HAp scaffolds was comparable to the empty defects and while the HAp scaffolds provided significant increase in modulus when compared to empty defect and their flexural toughness was comparable to autografts after 8 weeks of implantation.

T. Guda (✉) · J. A. Walker · J. C. Wenke
Extremity Trauma and Regenerative Medicine Task Area, United States Army Institute of Surgical Research, 3400 Rawley E. Chambers Ave., Fort Sam Houston, TX 78234, USA
e-mail: teja.guda@gmail.com

T. Guda · B. E. Pollot · M. R. Appleford · S. Oh · J. L. Ong
Department of Biomedical Engineering, The University of Texas at San Antonio, One UTSA Circle, San Antonio, TX 78249, USA

T. Guda
Wake Forest Institute of Regenerative Medicine, Wake Forest University Health Sciences, Richard H. Dean Biomedical Building, 391 Technology Way, Winston-Salem, NC 27157, USA

1 Introduction

An estimated 500,000 bone grafting procedures are performed annually in the US, with more than half of these procedures related to spinal fusion [1]. However, conventional use of autograft and allograft materials for these procedures carry the associated risk of donor site morbidity as well as disease transmission from allogeneic bone origin. Autologous grafts from the iliac crest remain the gold standard for small bone defects [2] but limited availability restricts their therapeutic use as bone fillers for treating non-unions, delayed unions, ostectomies and large segmental defects from bony loss due to neoplasia or cysts [3, 4]. This has led to a strong clinical need to develop synthetic material-based scaffolds as alternatives to autografts and allografts. Parameters that must be addressed during scaffold fabrication include material selection for promoting tissue regeneration and integration, graft architecture design for sustaining tissue in-growth as well as nutrient perfusion and transport, and scaffold strength for providing mechanical stability and functionality [5, 6].

Hydroxyapatite (HAp), a crystalline phase of calcium phosphate found naturally in bone minerals, has shown tremendous promise as a graft material. It exhibits initial mechanical rigidity and structure, and demonstrates osteoconductive as well as angiogenic properties in vivo [7–9]. Additionally, fabricated porous HAp scaffolds were reported to promote a strong mechanical interlock with

host bone tissue [7, 10, 11]. Since the extent of bony in-growth within the scaffold, the functionality of newly regenerative bone tissue, and the development of a vascularized network within the scaffolds are dictated by the porous scaffold architecture, extensive studies have been performed to optimize pore configurations needed for maximal bone tissue integration [12–14].

Greater in vitro cell proliferation was observed in smaller pore grafts as a result of higher surface area, whereas rapid in vivo bone infiltration was reported for scaffolds with high porosity and interconnectivity [14]. Scaffolds with pore sizes in the range of 300–500 μm were suggested to show greater bone forming efficiency in vivo, with new bone formation occurring directly into the pore spaces [12, 15–17]. However, the main disadvantage of having highly macroporous scaffolds is the reduced mechanical strength. Since an optimal range of both pore size and interconnectivity are essential to achieve both initial stabilization and long term bony integration, it has been recommended that scaffolds should contain gradients in pore sizes [18].

Previously, we demonstrated that open pore HAp scaffolds could be prepared by template coating to produce an open porous highly interconnected structure with a mean porosity of 77% [7]. In a canine mandible model in vivo, these scaffolds regenerated 7% of the defect at 3 weeks and 59% at 12 weeks [7]. It is hypothesized that increasing surface area of the scaffold would increase initial and progressive in-growth of bone.

Mimicking natural long bones, where there is an outer cortical and an inner trabecular layer, the in vivo biomechanical performance of bilayer HAp scaffolds was evaluated in this study. The fabricated bilayer HAp scaffolds consisted of a trabecular-like inner core with large interconnecting (>450 μm) pores to promote fluid transport and an outer cortical-like shell to provide mechanical stability through a denser design while maintaining interconnecting (~200 μm) pores. This design would also significantly increase scaffold surface area by incorporating smaller pore volumes on the periphery. Biomechanical stability, histological analyses and micro-computed tomography (Micro-CT) were performed on these scaffolds after 8 weeks implantation in a rabbit radius segmental defect model to test the hypothesis of better interfacial bone in growth for functional stabilization of a large defect as well as their overall bone regeneration capacity.

2 Materials and methods

2.1 Scaffold preparation

Using a previously described template coating process [7], bilayer HAp scaffolds were prepared. Briefly, a polyurethane sponge template (EN Murray, Denver, CO) for the trabecular cores was snuggly fit into a pipe-like polyurethane sponge template for the outer cortical shell, resulting in a one piece bilayer scaffold template. Mean template pore size for the outer dense shell (73% total volume) and inner porous core (27% total volume) was 200 and 450 μm, respectively. The templates were designed to mimic a 10 mm segmental defect in the rabbit radius model and had an elliptical cross-section to match the bone with a 5 mm major axis and a 3 mm minor axis. The one piece bilayer templates were then twice coated in distilled water-based HAp slurry. Binders used with the slurry to improve sintering and to stabilize the scaffold structure included 3% high molecular weight polyvinyl alcohol, 1% v/v carboxymethylcellulose, 1% v/v ammonium polyacrylate dispersant, and 3% v/v *N*,*N*-dimethylformamide drying agent. Coated sponges were then vacuum-dried overnight before sintering to 1,230°C for 3 h in a high temperature furnace (Thermolyne, Dubuque, Iowa). All scaffolds were sterilized using ethylene oxide gas sterilization prior to implantation.

2.2 Porosity measurement

Prior to animal study, the porosity of bilayer scaffolds was characterized using helium pycnometry (Accupyc 1340, Norcross, GA) to measure the true solid volume of the scaffold (V_{solid}). The length and diameter of each scaffold was determined by averaging three independent measurements per scaffold to calculate the volume of the bounding cylinder (V_{cyl}). This allowed computation of porosity as the void volume fraction using the equation

$$\text{Porosity } (\%) = \left(1 - \left(V_{solid}/V_{cyl}\right)\right) \times 100.$$

2.3 Animal surgery

A unilateral 10 mm segmental defect was created in the left radial diaphysis of 36 skeletally matured New Zealand White rabbits (Myrtles Rabbitry, Inc., Thompson Station, TN), of a minimum age of 1 year. This study has been conducted in compliance with the Animal Welfare Act, the implementing Animal Welfare Regulations and in accordance with the principles of the Guide for the Care and Use of Laboratory Animals. A 20 mm incision was made over the middle third of the radius. The overlying tissues were then dissected to expose the radial diaphysis where a 10 mm segmental defect was created with an oscillating saw, under copious irrigation with sterile normal saline. The defects either had no treatments (negative controls: Defect Group), were implanted with 10 mm scaffolds (experimental treatment: Scaffold Group), or implanted with autologous bone grafts (positive controls: Autograft Group) harvested from the iliac crest of

the same rabbit [19]. After scaffold or autologous bone graft implantation, internal fixation was not necessary because of the fibro-osseous syndesmosis between the ulna and radius. Immediately after implantation, the soft tissues were approximated with a continuous 2-0 Vicryl® (Ethicon Inc., Somerville, NJ) and the skin was closed with deep dermal stitches using a 3-0 Vicryl® (Ethicon Inc., Somerville, NJ). All animals were kept alive for 8 weeks post surgery.

2.4 Radiographic evaluation

Immediately following surgery, standardized radiographs were made of the defect limbs. Standardized radiographs were again made of the experimental limbs at 2, 4 and 6 weeks and at 8 weeks immediately after sacrifice.

2.5 Micro-CT evaluation

Following sacrifice, micro-CT analyses of all samples were performed prior to histology or mechanical testing. All samples were either wrapped in gauze hydrated with phosphate buffered saline (PBS) and preserved frozen post sacrifice or placed in formalin, depending on the type of testing after micro-CT evaluation. Micro-CT analysis was performed using Skyscan 1076 (Skyscan, Kontich, Belgium) at a 8.77 μm pixel resolution while hydrated with formalin or PBS. The images were reconstructed using NRecon software (Skyscan, Kontich, Belgium) to generate grayscale images ranging from 0 to 255 which was equivalent to the density range 0.81–3.34 gm/cm^3. The micro-CT reconstructed axial slices were then evaluated using CTAn software (Skyscan, Kontich, Belgium) to determine the bone regeneration patterns in vivo in terms of density, growth profiles and overall bone volume. The density of the new bone formed in the defect and the average density of the bone in the autograft group were evaluated. This was compared to the density of the regenerated bone within the scaffold, while excluding the HAp scaffold itself. New bone evaluation was based on differences in density between the scaffold (2.5 gm/cm^3 mean) and the newly forming osteoid or remodeling native bone (1.2–1.7 gm/cm^3). While the HAp scaffold could be separated in micro-CT evaluation from the regenerated bone, this was not possible for the autograft group and all the data reported for that group included both the regenerated bone as well as the remodeled autograft. The region of interest was a 3-D volume that extended over the 10 mm defect space created at the time of surgery. The bone area in each 8.77 mm section of this 10 mm defect space was computed for all three treatments to observe the trends in bone regeneration along the length of the defect: from the proximal to the distal interface. Total bone formed within the defect spaces was also measured, which included the calcified interosseous syndesmosis, but excluded the ulna.

2.6 Histological evaluation

Immediately following sacrifice, four excised radius and ulna per group were placed in formalin for histological evaluation. Bone-scaffold blocks were embedded in one-component photo-curing resin (Exakt 7200 VLC, Oklahoma City, OK), and thin sections of the bone-scaffold blocks were prepared using a precision microsaw (Buehler, Lake Bluff, IL). Sections were progressively polished to 1,200 grit paper and adhered to glass slides using a methyl methacrylate resin (Surgipath Medical Ind., Richmond, IL). The sections were stained for connective tissues with Paragon (toluidine blue and basic fuchsin) and calcified bone tissue with Alizarin Red, followed by imaging at 40× magnification with a digital camera (QImaging, Burnaby, Canada) on a Nikon TE300 microscope (Leica Microsystems GmbH, Wetzlar, Germany). Mineralized bone was stained red with Alizarin Red, whereas fibrous tissues were stained purple with Paragon, and the HAp scaffolds were opaque and appear blue/black.

2.7 Biomechanical evaluation

Immediately following sacrifice, eight excised radius and ulna per group were wrapped in gauze hydrated with PBS and preserved frozen for mechanical testing. The radius and ulna were cut to a 26 mm length centered about the defect while preserving the interosseous membrane since micro-CT analysis showed significant bone ingrowth into the scaffolds from the fibro-osseous syndesmosis. The corresponding sites on the intact contralateral limbs were excised to serve as controls for the biomechanical evaluation. The specimens were tested to flexural failure in a four point bending configuration with a 10 mm spacing between the loading supports and a 20 mm spacing between the base supports. The specimens were loaded in dorsal–ventral orientation at a constant strain rate of 0.5 mm/min on an Insight 5 uniaxial test frame (MTS Systems Corp., Eden Prairie, MN). Flexural modulus and peak flexural strength were measured, and flexural toughness was computed as the total energy observed. The moment of inertia of the specimen was calculated from the micro-CT images using the CTAn software package.

2.8 Bone mineral evaluation

Following mechanical testing, 6 mm sections from the mid-diaphysis of the contralateral forearms from all three groups were sectioned and ashed in a Thermolyne 48000 muffle furnace (Barnstead/Thermolyne Corporation, Dubuque, IA) at 600°C for 24 h. The ashed samples were then weighed and their volume measured using helium pycnometry, as described previously to measure absolute

mineral density (specific gravity of the mineral). Since the true volume of the ashed bone is used in this calculation, it is comparable to the absolute density of the mineral phase. Chemically pure hydroxyapatite on this scale had a value of 3.08 gm/cm^3. The ashed samples were then cut in half along the long axis of the ulna. Under a JCM-5700 scanning electron microscope (Jeol Ltd., Tokyo, Japan), energy dispersive spectroscopy was performed on the outer cortical and intramedullary surfaces and calcium to phosphorus (Ca/P) ratios were calculated.

2.9 Statistical analysis

All data is reported as mean ± standard error of the mean. Significance in micro-CT and mineral density measures reported was determined using one way ANOVA and Tukey's test for post hoc evaluation. Significance in biomechanical evaluations and Ca/P ratios was determined using a two way ANOVA and Tukey's test for post hoc evaluation. Paired *T*-test analysis was performed between defect and contralateral limbs from the same animal, with significance levels set at $P < 0.05$ for all statistical measures reported.

3 Results

3.1 Porosity measurement

With specific gravity of HAp computed at 3.04 g/cm^3, helium pycnometry indicated a mean scaffold porosity of 65.32 ± 3.99% prior to animal implantation.

3.2 Radiographic evaluation

Representative radiographs showing surgically cut bone interfaces are seen for defects receiving no treatments, defects implanted with scaffolds and defects implanted with autologous bone grafts immediately after surgery (week 0 in Fig. 1). In the defect group, it is easy to observe in the weeks post-surgery, that the representative radiographs show new bone formation, with no bridging at defect sites. Evidence of new bone formation at the scaffold bone interface was observed for defects implanted with scaffolds and good integration was observed at the interfaces in the scaffold treatment group at 8 weeks (Fig. 1). For defects implanted with autologous bone grafts, bridging of the defects was observed with woven and mature bone spanning the defect site and the newly formed bone was indistinguishable from the implanted autologous graft (Fig. 1). Bone formation in all defects was observed from three distinct fronts of bone formation, that is, from the proximal interface, from the distal interface, and from the interosseous syndesmosis that spans from the ulna to the radius. However, these three distinct fronts of bone formation were more clearly exhibited in defects with no treatment.

3.3 Micro-CT evaluation

Micro-CT analysis indicated new bone formation and bone in-growth within the scaffolds, including regions in the interior of the scaffolds away from the interfaces after 8 weeks post surgery (Fig. 2). Micro-CT sections showed conical growth fronts from the interfaces in defects with no

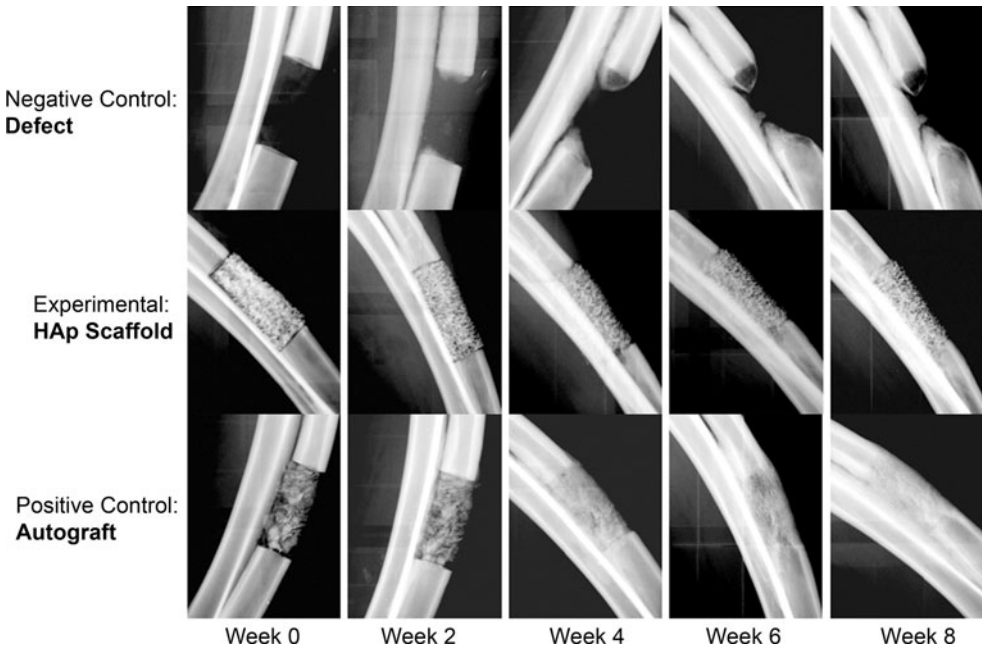

Fig. 1 Defect with no scaffold as negative control (*row 1*), defect with the HAp bilayer scaffold (*row 2*), and defect with autologous bone graft as the clinical control (*row 3*) at immediately after surgery, and weeks 2, 4 and 6 while animals were in veterinary care and at 8 weeks immediately after sacrifice

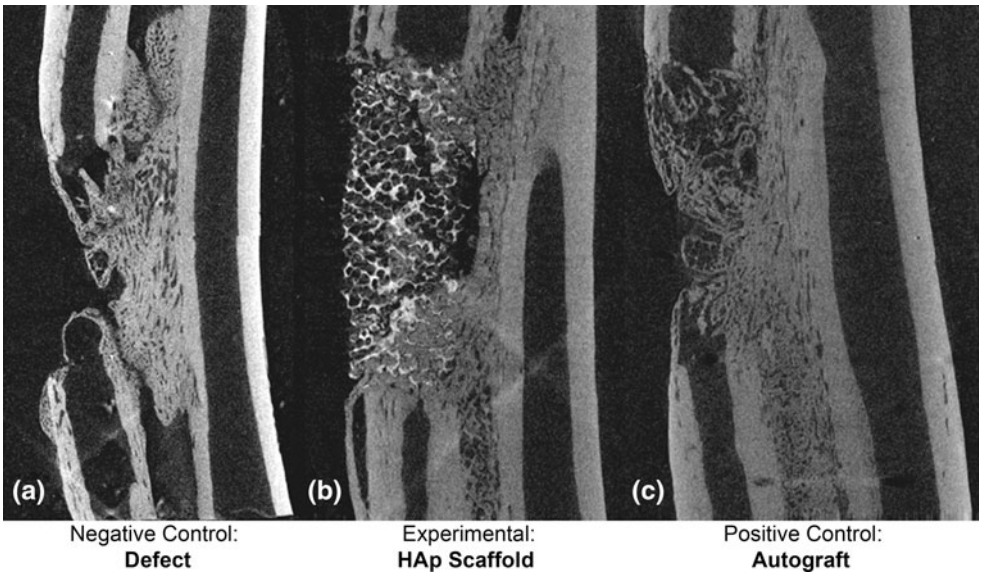

Fig. 2 Micro-CT evaluation showing bone regeneration and remodeling in the defect (**a**), experimental scaffold (**b**) and autologous graft groups (**c**) in the coronal longitudinal sections through the rabbit fore-arm

treatments (Fig. 2a), good interfacial integration in defects implanted with scaffolds (Fig. 2b) and bridging across the defect space with no distinction between graft and new bone formation in defects implanted with autologous bone grafts (Fig. 2c). Extensive ossification from the interosseous membrane was also seen within HAp scaffolds, with ossified callus formation around the scaffold periphery in some cases.

The bone mineral density was significantly greater in the autograft group when compared to the regenerated bone in the empty defect ($P < 0.0001$) and scaffold treatments ($P < 0.0001$) (Fig. 3a). However, in the case of the autograft this density measure included the mineral density of the autologous bone graft initially placed in the defect that had remodeled over 8 weeks since this could not be distinguished from the regenerated bone using micro-CT, while the HAp scaffold itself was excluded from this density metric. Taking into account all ossified tissue (excluding the ulna and scaffold material if any but including the syndesmosis) in the 10 mm defect length at 8 weeks after surgery, Fig. 3b indicated no statistically significant difference between the total regenerated bone volume between the empty defect and within the HAp scaffold. The total volume of the HAp scaffold + regenerated bone was significantly greater than the bone volume in the defect group but less than the total bone volume of the autograft treatment.

An evaluation of the patterns of bone regeneration and remodeling within the 10 mm defect space, carried out by computing the mean cross sectional bone area in each micro-CT slice for virtual histology every 8.77 μm showed that the bone area at each location along the defect was less than the total area of bone and scaffold in the HAp treatment which in turn was lesser than the bone area in the

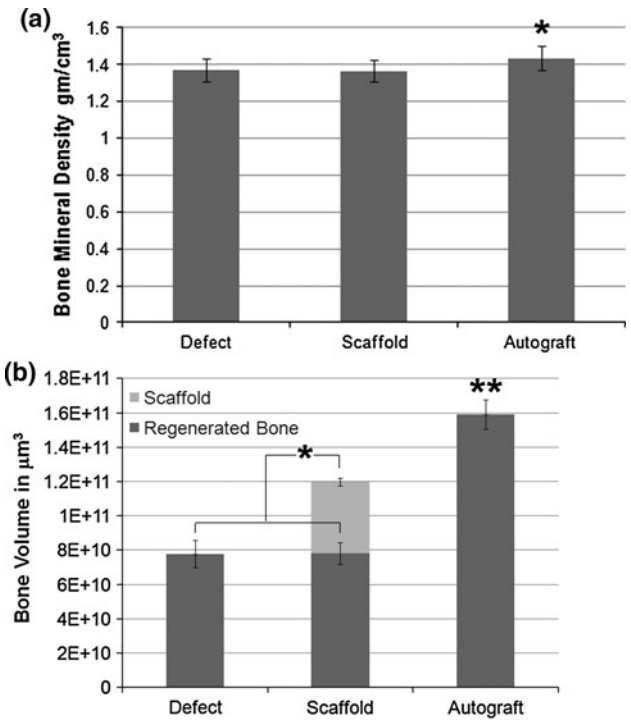

Fig. 3 **a** The mineral density of the regenerated bone in the defect and within the scaffold and all the bone present in the autograft group was assessed for bone quality. **b** The total volume of the regenerated bone in the defect, HAp scaffold and in the autograft treatment was calculated for bone quantity

autograft group (Fig. 4a). A comparison of the cross sectional area of the regenerated bone alone in the defect and HAp treatments (excluding the scaffold area) showed almost identical patterns of bone regeneration (Fig. 4b) in the two treatments.

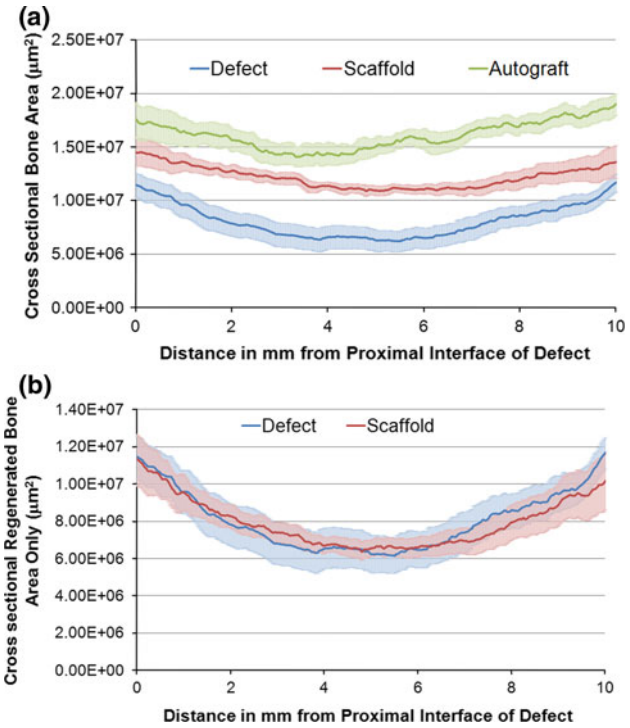

Fig. 4 **a** The cross sectional bone (including scaffold) area (mean ± SEM) was plotted every 8.7 μm across the 10 mm space created from the proximal (0) to the distal (10) interface to assess bone regeneration and remodeling trends for the three treatment groups (Autograft > Scaffold > Defect). **b** The cross sectional bone area (scaffold itself excluded) along the 10 mm space in the defect and scaffold groups showing almost identical trends in regeneration

3.4 Histological evaluation

Histological evaluation of defects with no treatments showed that the conical bone growth fronts from the interfaces were hollow (Fig. 5a), suggesting in-growth primarily from the cortical bone. Connective tissue encapsulation in defects with no treatments and the presence of periosteal callus-like layer surrounding defects with scaffold implantation were observed after 8 weeks post surgery (Fig. 5a, b). Under phase contrast microscopy, defects implanted with scaffolds were observed to be infiltrated at the bone-scaffold interface with mineralized bone tissue within the scaffolds (Fig. 5b). The connective tissue formed within the scaffolds was vascularized, with very few acellular regions observed. Newly formed osteoid was also observed adjacent to the scaffolds. Additionally, at selected regions of the defects implanted with scaffolds (Fig. 5b), adipose tissue was found infiltrating the scaffold regions corresponding to the original marrow cavity of the radius, whereas such adipose tissue was found interspersed with mature bone tissue in defects implanted with autologous bone grafts (Fig. 5c).

3.5 Biomechanical evaluation

As shown in Fig. 6a, the comparison of the experimental treatments shows that the flexural strength of the autologous bone graft (43.84 ± 15.31 MPa) was significantly greater ($P < 0.001$) than the flexural strength of the empty defects (16.13 ± 7.81 MPa) and the implanted scaffolds (26.59 ± 6.96 MPa). Surprisingly, the flexural strength of contralateral limbs for animals in the autologous bone graft group was significantly greater ($P < 0.001$) when compared to contralateral limbs for animals in the defect group or HAp scaffolds treatment group (Fig. 6a).

No significant difference in flexural modulus was observed when comparing both the experimental limbs as well as with the contralateral limbs for the different treatments. The flexural modulus for the experimental groups

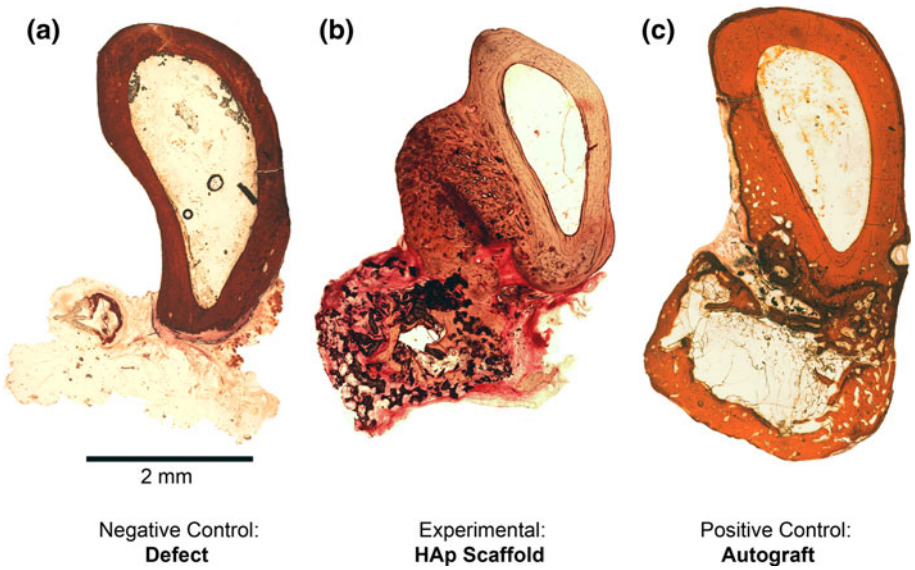

Fig. 5 Bone tissue cross sections at 8 weeks post surgery, stained with Paragon violet for connective tissue (*light*) and Alizarin Red for mineralized bone tissue (*dark*), showing **a** very little bone formation and significant connective tissue in the defect, **b** regeneration and growth infiltrating the scaffold (*black*) and **c** organized formation of cortex like bone in the autograft. (*Grayscale levels in brackets*)

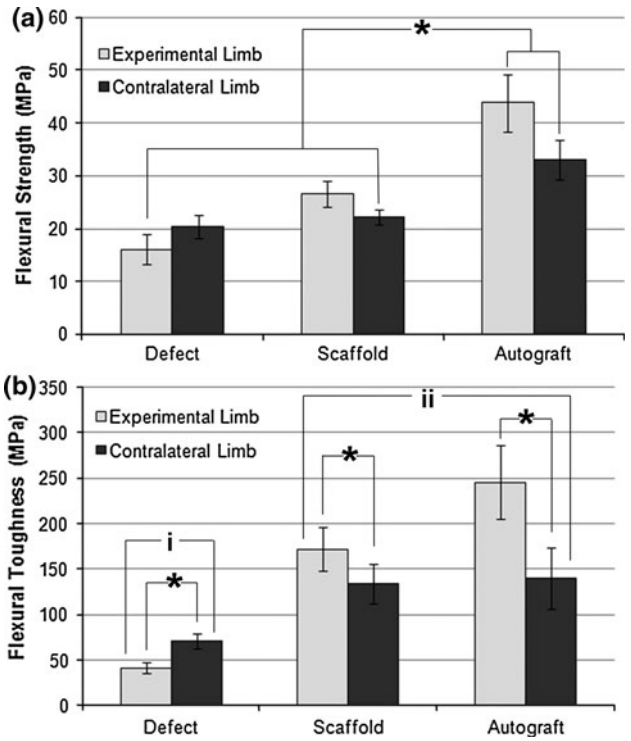

Fig. 6 Flexural strength (**a**) and flexural toughness (**b**) of the experimental limb and the contralateral limb of the rabbit in the defect, HAp scaffold and auto-graft treatment groups were measured after 8 weeks in vivo

was: 489 ± 97 MPa for the defect, 737 ± 119 MPa for the scaffold and 795 ± 68 MPa for the autograft. The flexural modulus for the contralateral limbs was 826 ± 75 MPa for the defect, 882 ± 97 MPa for the scaffold and 750 ± 81 MPa for the autograft. No significant difference in the flexural toughness was observed for experimental limbs implanted with scaffolds and autologous bone grafts, whereas a significantly lower flexural toughness ($P < 0.001$) was observed from experimental limbs in the defect group (Fig. 6b). A significantly different flexural toughness was also observed when comparing the defect limbs to the contralateral limbs of the same treatment (Fig. 6b). The contralateral limbs of animals in the defect group were observed to have significantly higher flexural toughness when compared to experimental limbs ($P < 0.004$). In contrast, a significantly higher flexural toughness was observed for the experimental limbs of animals receiving scaffolds ($P < 0.025$) or autologous bone graft treatments ($P < 0.002$) when compared to the contralateral limbs of the respective treatment groups.

In comparing the experimental limbs of animals implanted with scaffolds to their contralateral limbs at 8 weeks post surgery, mean flexural strength and flexural modulus of the scaffold implanted defects were observed to have 121.5 ± 33.8 and 90.7 ± 49.2% recovery, respectively. Failure at the bone-scaffold interface was observed for 50% of the experimental limbs implanted with scaffolds whereas the remaining 50% of the defect limbs implanted with scaffolds failed within bone, with all failures showing a short oblique fracture through the intact bone of the radius well away from the interface. Additionally, the interosseous membrane was observed to be the first location of failure for six of the eight scaffolds tested. For animals implanted with autologous bone graft, six out of eight experimental limbs failed via a short oblique crack at an interface, whereas the remaining two limbs failed at the interosseous membrane.

3.6 Bone mineral evaluation

The absolute mineral density of contralateral limbs for animals receiving no treatments was significantly lower ($P < 0.026$) when compared to the mineral density of contralateral limbs for animals receiving scaffolds or autologous bone grafts treatments (Fig. 7a). In agreement with the mineral density observations, Fig. 7b shows that the intramedullary surfaces on the contralateral ulna for animals receiving no treatments have a significantly lower Ca/P ratio of 1.06 ± 0.05 ($P < 0.003$) when compared to the intramedullary surfaces on the contralateral ulna for

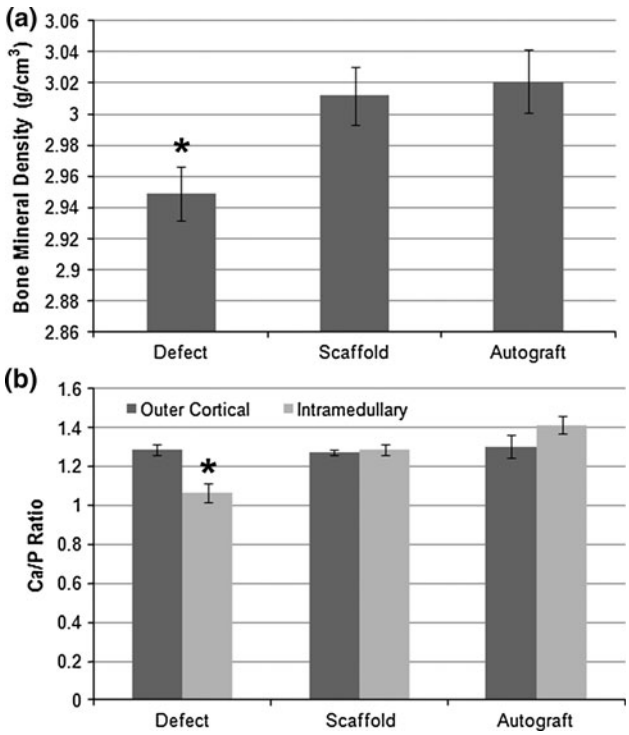

Fig. 7 Mineral density (**a**) of the non-experimental contralateral limb in the defect group was significantly lower than the corresponding contralateral limb in the scaffold and autograft groups. EDX measurement showed a correspondingly lower intra-medullary Ca/P ratio (**b**) in the defect contralaterals

animals receiving scaffolds (1.29 ± 0.03) and autologous bone graft (1.41 ± 0.05) treatments. No significant difference in Ca/P ratio was observed for the outer cortical region of the contralateral ulna for animals of the three treatment groups (1.29 ± 0.02).

4 Discussion

Taking an organizational cue from human bone, the in vivo performance of bilayer HAp scaffolds having distinct cortical-like and trabecular-like architectures were evaluated in this study. It was rationalized that the denser cortical-like shell would provide adequate mechanical strength and that the more porous core would allow bone integration. The integrated scaffold, as observed by new bone growth within the scaffold interfaces, along with significant connective tissue encapsulation, provided adequate strength that closely matched intact bone. Significant differences have been observed in the nature and extent of bone in-growth depending on whether the scaffolds were in contact with cortical, trabecular or medullary bone [20]. The relative in vivo osteoid volume was observed to be greater near the medullary sites at 12 weeks after surgery and near the cancellous sites at 24 weeks after surgery [20]. While porous ceramics have been shown to support new bone formation into the pore spaces at 6 and 12 weeks after implantation [7], significantly more bone were reported near the cortex as opposed to the canal at 36 and 52 weeks in vivo [19]. It was observed from the histological and micro-CT evaluations performed in this study that new bone was formed at bone-scaffold interfaces as well as from contact locations with the interosseous membrane. Additionally, micro-capillaries were observed within the new bone tissue and the connective tissue layer was highly vascularized.

Micro-CT data in this study also indicated that the HAp scaffold did not impede bone growth at any location in the 10 mm defect space created when compared to the empty defects with no treatment, showing the true osteoconductive nature of the scaffold material. Considering that the scaffold maintains open porosity allowing bone ingrowth with equivalent bone volume regenerated to an empty defect space suggests the possible application of this scaffold as an ideal carrier for either cells or growth factors to further improve bone formation. It should be noted that although significant bone regeneration was observed in the empty controls with no treatment, bridging of the defect was not observed in this segmental model at 8 weeks and that all treatment groups need to be studied at longer time points to assess true regeneration potential.

The biomechanical evaluation performed in this study indicated initial failure at the interosseous membrane, suggesting a strong load sharing mechanism through this syndesmosis between the radius and the ulna. The syndesmosis was shown to have extensive calcification, accounting for a large fraction of the bone volume in the defect and possibly contributed to the bone in-growth into the scaffold. This was supported both by micro-CT measurements and radiographic evidences showing new bone growth in a cone-like fashion and from the direction of the interosseous membrane in defects implanted with scaffolds as well as in defects with no treatments. Thus, separating the radius from the ulna for biomechanical testing may damage this tissue. It is also important to consider that the radius and ulna acts as a unit in the physiological setting and that it may be more biologically-relevant to evaluate them together.

To evaluate mechanical recovery of bone grafts in the rabbit radius segmental defect model, a variety of test configurations have been reported including bending [21–23], torsion [21, 24], and compression [25]. Recent studies have shown that both four point bending and torsion resulted in similar outcomes when testing the mechanical integrity of rabbit radius [21]. In agreement with this study, the primary failure mode for bending was a short oblique fracture, whereas the failure mode for torsion testing was a spiral fracture [21]. Additionally, the reported primary failure zone was constrained to the location of the central contact in the three point bending while the four point mode was reported to have a more uniform stress distribution within the central loading span [26]. Since the objective of this study was to evaluate the interfacial integration of the scaffold to the bone, a four point bending testing was chosen, with the scaffold lying completely within the loading span. Other confounding factors such as loading to support span ratios, contact geometry and load rates were matched to suggestions in literature [26]. The four point bending test is as such a physiologically relevant shear loading mode for fracture in this limb.

In this study, the observed mean strength of the defect limbs containing scaffolds was 121.5 ± 33.8% of its contralateral limbs after 8 weeks implantation. Using a three point bend test for radius defects implanted with chitosan-coated calcium sulfate scaffolds, other investigators showed a 20–50% recovery in flexural strength compared to contralateral radii [22]. While relative recovery from contralateral limbs has been commonly reported, the combined use of micro-CT calculations of true area moments of inertia performed in this study allowed for the calculation of true flexural stress, modulus and toughness in addition to peak load carried in the limb. Flexural toughness is the energy absorbed prior to failure and thus carries physiological relevance in terms of effective bone stability. Additionally, no significant difference in flexural modulus was observed when comparing the experimental limbs with different

treatments as well as comparing the contralateral limbs of animals receiving different treatments.

Significant differences in flexural toughness were observed, with the contralateral limbs of animals with no treatments were observed to have significantly lower flexural toughness when compared to the contralateral limbs of animals receiving scaffolds or autologous bone graft treatments. Similarly, the absolute mineral density and the Ca/P ratio of intermedullary surfaces on the contralateral limbs for animals receiving no treatments were significantly lower when compared to the absolute mineral density and the Ca/P ratio of intermedullary surfaces on the contralateral limbs for animals receiving scaffolds or autologous bone grafts treatments. Although the rabbit radius defect is a widely used animal model to test bone regeneration, and bone mineral density was often reported from radiographic data as a measure of tissue healing [27, 28], this is the first study to report changes in bone mineral composition at other anatomical sites during the fracture healing process. However, the effect of the HAp scaffolds and autologous bone grafts to maintain absolute mineral density and Ca/P ratios at distant bone sites, as observed in the diaphyses of the contralateral bones in this study, bears further investigation in the futures since maintaining calcium homeostasis [29] is also a function of the normal skeleton.

Additionally, it is also possible that connective tissue callus may have contributed to the mechanical stabilization of the scaffold and the extent of load carried through the radius. From histological and micro-CT evaluations performed in this study, the relatively dense encapsulation was observed to be a highly organized structure containing densely packed strand-like collagen bundles. Since pure ceramics have low energy absorption to failure and high stiffness, the observation of relatively higher flexural toughness in the scaffolds as compared to intact bone which was also comparable to the toughness of autologous graft material also supported the role played by the connective tissues in enhancing the stability of scaffolds implanted in the defect sites.

5 Conclusions

This study suggests that the HAp scaffolds can serve as an ideal scaffold carrier platform for bone regeneration because they do not impede bone formation, add to the strength and toughness of the defect site, and may reduce deleterious effects on the skeleton during the healing process.

New bone in-growth in defects was promoted with the implantation of bilayer HAp scaffolds, with total regenerated bone volume being comparable to empty defects and flexural toughness being comparable to defects implanted with autologous bone grafts. The scaffolds also promoted the presence of connective tissue encapsulation around the scaffolds, thereby possibly contributing to the stability of the implanted scaffolds. Additionally, it was also concluded that the therapeutic effect of HAp scaffold implantation was comparable to autologous bone graft implantation in defects with respect to the maintenance of mineral density and intramedullary Ca/P ratios at distant bone sites.

Acknowledgments This study was supported in part by the Department of Defense funds and the Orthopaedic Extremity Trauma Research Program grants (USAMRMC # W81XWH-08-1-0393 and W81XWH-07-1-0717). The opinions or assertions contained herein are the private views of the author and are not to be construed as official or as reflecting the views of the Department of the Army or the Department of Defense.

References

1. Greenwald AS, Boden SD, Goldberg VM, Khan Y, Laurencin CT, Rosier RN. Bone-graft substitutes: facts, fictions, and applications. J Bone Joint Surg Am. 2001;83-A:98–103.
2. Giannoudis PV, Dinopoulos H, Tsiridis E. Bone substitutes: an update. Injury. 2005;36:S20–7.
3. Glancy GL, Brugioni DJ, Eilert RE, Chang FM. Autograft versus allograft for benign lesions in children. Clin Orthop Relat Res. 1991;262:28–33.
4. Laurie SW, Kaban LB, Mulliken JB, Murray JE. Donor-site morbidity after harvesting rib and iliac bone. Plast Reconstr Surg. 1984;73(6):933–8.
5. Guda T, Appleford M, Oh S, Ong JL. A cellular perspective to bioceramic scaffolds for bone tissue engineering: the state of the art. Curr Top Med Chem. 2008;8(4):290–9.
6. Oh S, Oh N, Appleford M, Ong JL. Bioceramics for tissue engineering applications—a review. Am J Biochem Biotechnol. 2006;2(2):49–56.
7. Appleford MR, Oh S, Oh N, Ong JL. In vivo study on hydroxyapatite scaffolds with trabecular architecture for bone repair. J Biomed Mater Res A. 2009;89(4):1019–27.
8. Kilian O, Wenisch S, Karnati S, Baumgart-Vogt E, Hild A, Fuhrmann R, et al. Observations on the microvasculature of bone defects filled with biodegradable nanoparticulate hydroxyapatite. Biomaterials. 2008;29(24–25):3429–37.
9. Yoshikawa T, Ohgushi H, Nakajima H, Yamada E, Ichijima K, Tamai S, et al. In vivo osteogenic durability of cultured bone in porous ceramics: a novel method for autogenous bone graft substitution. Transplantation. 2000;69(1):128–34.
10. Costantino PD, Friedman CD, Jones K, Chow LC, Pelzer HJ, Sisson GA Sr. Hydroxyapatite cement. I. Basic chemistry and histologic properties. Arch Otolaryngol Head Neck Surg. 1991;17(4):379–84.
11. Ohgushi H, Dohi Y, Tamai S, Tabata S. Osteogenic differentiation of marrow stromal stem cells in porous hydroxyapatite ceramics. J Biomed Mater Res. 1993;27(11):1401–7.
12. Kuboki Y, Jin Q, Takita H. Geometry of carriers controlling phenotypic expression in BMP-induced osteogenesis and chondrogenesis. J Bone Joint Surg Am. 2001;83-A:S105–15.
13. Martin RB, Chapman MW, Sharkey NA, Zissimos SL, Bay B, Shors EC. Bone ingrowth and mechanical properties of coralline hydroxyapatite 1 yr after implantation. Biomaterials. 1993; 14(5):341–8.

14. Mastrogiacomo M, Scaglione S, Martinetti R, Dolcini L, Beltrame F, Cancedda R, et al. Role of scaffold internal structure on in vivo bone formation in macroporous calcium phosphate bioceramics. Biomaterials. 2006;27(17):3230–7.
15. Daculsi G, Passuti N. Effect of the macroporosity for osseous substitution of calcium phosphate ceramics. Biomaterials. 1990;11:86–7.
16. Gauthier O, Bouler JM, Aguado E, Pilet P, Daculsi G. Macroporous biphasic calcium phosphate ceramics: influence of macropore diameter and macroporosity percentage on bone ingrowth. Biomaterials. 1998;19(1–3):133–9.
17. Shimazaki K, Mooney V. Comparative study of porous hydroxyapatite and tricalcium phosphate as bone substitute. J Orthop Res. 1985;3(3):301–10.
18. Karageorgiou V, Kaplan D. Porosity of 3D biomaterial scaffolds and osteogenesis. Biomaterials. 2005;26(27):5474–91.
19. Stubbs D, Deakin M, Chapman-Sheath P, Bruce W, Debes J, Gillies RM, et al. In vivo evaluation of resorbable bone graft substitutes in a rabbit tibial defect model. Biomaterials. 2004; 25(20):5037–44.
20. Lu JX, Gallur A, Flautre B, Anselme K, Descamps M, Thierry B, et al. Comparative study of tissue reactions to calcium phosphate ceramics among cancellous, cortical, and medullar bone sites in rabbits. J Biomed Mater Res. 1998;42(3):357–67.
21. Bowers KW, Edmonds JL, Girod DA, Jayaraman G, Chua CP, Toby EB. Osteocutaneous radial forearm free flaps. The necessity of internal fixation of the donor-site defect to prevent pathological fracture. J Bone Joint Surg Am. 2000;82(5):694–704.
22. Cui X, Zhang B, Wang Y, Gao Y. Effects of chitosan-coated pressed calcium sulfate pellet combined with recombinant human bone morphogenetic protein 2 on restoration of segmental bone defect. J Craniofac Surg. 2008;19(2):459–65.
23. Shafiei Z, Bigham AS, Dehghani SN, Nezhad ST. Fresh cortical autograft versus fresh cortical allograft effects on experimental bone healing in rabbits: radiological, histopathological and biomechanical evaluation. Cell Tissue Bank. 2009;10(1):19–26.
24. Mori M, Isobe M, Yamazaki Y, Ishihara K, Nakabayashi N. Restoration of segmental bone defects in rabbit radius by biodegradable capsules containing recombinant human bone morphogenetic protein-2. J Biomed Mater Res. 2000;50(2):191–8.
25. Kaito T, Myoui A, Takaoka K, Saito N, Nishikawa M, Tamai N, et al. Potentiation of the activity of bone morphogenetic protein-2 in bone regeneration by a pla-peg/hydroxyapatite composite. Biomaterials. 2005;26(1):73–9.
26. Draper ER, Goodship AE. A novel technique for four-point bending of small bone samples with semi-automatic analysis. J Biomech. 2003;36(10):1497–502.
27. Liu Y, Lu Y, Tian X, Cui G, Zhao Y, Yang Q, et al. Segmental bone regeneration using an rhBMP-2-loaded gelatin/nanohydroxyapatite/fibrin scaffold in a rabbit model. Biomaterials. 2009;30(31):6276–85.
28. Wu T, Nan K, Chen J, Jin D, Jiang S, Zhao P, et al. A new bone repair scaffold combined with chitosan/hydroxyapatite and sustained releasing icariin. Chin Sci Bull. 2009;54(17):2953–61.
29. Issa JPM, Bentley MVLB, Iyomasa MM, Sebald W, Albuquerque RFD. Sustained release carriers used to delivery bone morphogenetic proteins in the bone healing process. Anat Histol Embryol. 2008;37(3):181–7.